Journal of The Electrochemical Society, 2022 **169** 020506

Effects of Salt Aggregation in Perfluoroether Electrolytes

Brandon L. Peters, Zhou Yu, Paul C. Redfern, Larry A. Curtiss,[z] and Lei Cheng[z]

Joint Center for Energy Storage Research and Materials Science Division, Argonne National Laboratory, Lemont, Illinois 60439, United States of America

Electrolytes comprised of polymers mixed with salts have great potential for enabling the use of Li metal anodes in batteries for increased safety. Ionic conductivity is one of the key performance metrics of these polymer electrolytes and achieving high room-temperature conductivity remains a challenge to date. For a bottom-up design of the polymer electrolytes, we must first understand how the structure of polyelectrolytes on a molecular level determines their properties. Here, we use classical molecular dynamics to study the solvation structure and ion diffusion in electrolytes composed of a short-chain perfluoroether with LiFSI or LiTFSI salts. Density functional theory is also used to provide some insights into the structures and energies of the salt interactions with the perfluoroether. We observe the formation of aggregates of salts in the fluorinated systems even at low salt concentrations. The fluorine-fluorine attraction in the solvent is the governing factor for creating the salt aggregates. The aggregates' size and lifetime change with concentration and anion. These simulations provide an insight into the structure and dynamics of perfluoroether based electrolytes that can be used to improve Li-ion batteries.

 [DOI: 10.1149/1945-7111/ac4c7a]

Manuscript submitted November 4, 2021; revised manuscript received January 11, 2022. Published February 1, 2022.

Supplementary material for this article is available online

One of the mitigation strategies to address the climate challenge is the development and integration of energy storage for transportation and grid applications.[1–3] Although Li-ion batteries are the leader in battery-powered vehicles, there needs to be a reduction of capital costs, improvement in performance and life cycle, as well as safety.[4,5] Traditional liquid electrolytes based on organic compounds have stability issues due to the flammability and side reactions causing device damage.[6,7] Solid electrolytes may be a solution for some of these issues, and polymer-based electrolytes are serious contenders for solid electrolytes.

Polyethylene oxide (PEO) is an ether-based solid electrolyte that is stable with lithium[8] and PEO-based electrolytes have been studied extensively. However, these electrolytes still have low conductivity[8] at room temperature. Recently, groups have been developing fluorinated electrolytes as both additives[9] and as solvents,[7,10,11] due to their high voltage stability (up to 5.6 V for solvents[11]), which is larger than alkyl carbonates.[2] However, perfluoroethers have poor solubility for salts and, therefore, poor conductivity.[12] Little is known about the interactions between cation, anion, and the fluorinated solvent in these systems.[12] Grundy et al.,[7] hypothesize that there is a percolating network-like structure within the fluorinated solvent, while the papers on fluorinated additives do not mention percolating network structures.[13,14]

Molecular dynamics (MD) simulation is a great tool to understand the structure and dynamics of these electrolytes. Fluorinated solvents[15,16] and additives[13,14] have been examined via molecular dynamic simulations showing "clusters" of salts, but there has not been a detailed analysis on structure or transport properties of these clusters. However, it is noted, the effects of clusters on transport properties have been examined for PEO systems.[17] We make a distinction between clusters of ions in PEO systems[18,19] compared to the network structures (or salt aggregates). This means we examine aggregates of many lithium cations and anions (up to approximately 50 lithium cations and anions) compared to the anion-cation (one or two lithium cations) clustering.[17] The former has been defined in previous works by Molinari[19,20] et al. for highly concentrated PEO systems.

Here, we explore the structure and dynamics of electrolytes based on a fluorinated ether solvent and compare these properties with a tetraglyme electrolyte. The tetraglyme system showed an isotropic distribution of the lithium and anions, while the system with the perfluoropolyether solvent shows aggregation of the salts. We also compare the aggregate structures of LiTFSI and LiFSI in the fluorinated solvent and correlate these differences with the calculated transport properties of the electrolytes. Finally, we use density functional calculations to provide insight into the energetics of the systems.

Methods

We have performed classical molecular dynamics simulations using the OPLS force field[21] with a mixture of lithium ions, bis (trifluoromethanesulfonyl)imide (TFSI),[22] methyl carbonate terminated perfluoropolyether referred to as c8-dmc,[23] and tetraglyme.[24] The structures of these species are shown in Fig. 1. We used Gromacs 2019 simulation software[25] and the LigParGen to create the force field parameters.[26] The system contains 500 tetraglyme or c8-dmc chains with various concentrations of the LiTFSI. The fraction of salt molecules in the systems is, $x_{salt} = 0.03, 0.13, 0.24, 0.33, 0.41$. However, the LiTFSI concentration is best described as the ratio between lithium and oxygen in the chain. We examined the following concentrations: $r = [Li]/[O] = 0.003, 0.02, 0.03, 0.06$, and 0.08 for c8-dmc and $r = [Li]/[O] = 0.01, 0.03, 0.06, 0.09$, and 0.14 for tetraglyme.

We randomly assigned the chains in the simulation box, followed by the anion, and lastly, the lithium. The systems were then subjected to 1400 steps of steepest descent energy minimization to remove high-energy atomic overlaps, followed by 200 ns of molecular dynamics simulation at $T = 400$ K and $P = 1$ bar to accelerate structural relaxation. Lastly, 4 μs production runs were performed at $T = 300$ K and $P = 1$ bar. Equations of motion were integrated using the leapfrog algorithm with a time step of 2 fs. [27] Temperature control was done using a modified Berendsen thermostat[28] and pressure with the Parrinello-Rahman barostat.[29] Lennard-Jones interactions were switched smoothly to zero at a 1.2 nm cutoff and dispersion interactions between unlike atoms specified by Lorentz-Berthelot combining rules.[30] Electrostatics were treated using particle-mesh Ewald with a real-space cutoff of 1.2 nm and a reciprocal space grid spacing of 0.16 nm,[31] without any charge scaling. In Fig. 2 we show the tetraglyme and c8-dmc systems final snapshot with the solvent removed for clarity.

We also carried out DFT calculations on structures and binding energies of Li^+, FSI^-, and $Li(FSI)_2^-$ to various sites on c8-dmc to provide insight into the relative strengths of the interaction and for comparison to the MD results. In addition, we compare similar DFT

[z]E-mail: curtiss@anl.gov; leicheng@anl.gov

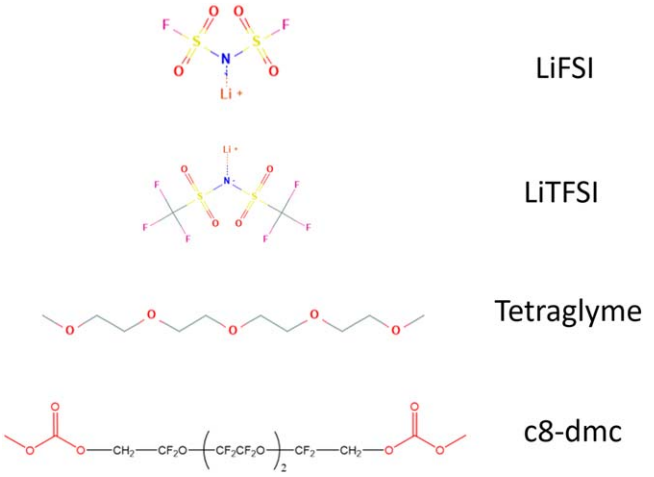

Figure 1. Structures of LiFSI, LiTFSI, tetraglyme, and c8-dmc.

results for PEO with triglyme as a model. The DFT studies were carried out using the B3LYP functional with optimizations done with the B3LYP/6–31 G(d) basis set and single-point energies calculated at these geometries with the 6–31 + G(d) basis set.[32]

Here, we use a single-linkage cluster algorithm to define aggregate structures, developed by Everitt et al.[33] and as employed by Yu et al.[34] The algorithm starts with an oxygen atom on the anion and then searches for another oxygen on the anion within or a lithium cation. Once the new oxygen or lithium is found, the search is repeated until there are no new oxygens or lithium's within the cutoff. More details can be found in Yu et al.[34]

The diffusion of a three-component system needs to be performed carefully. Initially, the self-diffusion of the three components is done by calculating the mean squared displacement as seen here,

$$MSD = \frac{1}{N}\sum_{i}^{N}\langle[\boldsymbol{r}_i(t) - \boldsymbol{r}_i(0)]^2\rangle \quad [1]$$

and then the diffusion constant was calculated through the Einstein's diffusion equation:

$$D = \frac{1}{6t}\lim_{t\to\infty}\langle[\boldsymbol{r}_i(t) - \boldsymbol{r}_i(0)]^2\rangle \quad [2]$$

To characterize the motion of the aggregates, we calculated the lifetime of salt aggregates. Here, we calculated the correlation function as in Borodin et al.[35] as seen here:

$$\mathrm{C(t)} = \frac{\langle h(t)h(0)\rangle}{\langle h(0)h(0)\rangle} \quad [3]$$

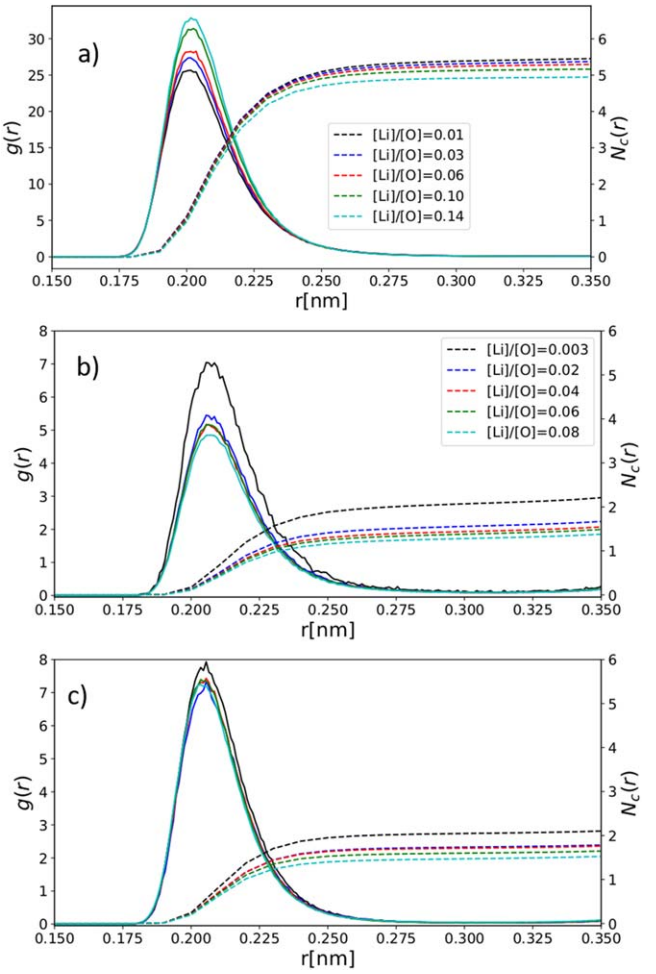

Figure 3. Radial distribution functions ($g(r)$) and coordination numbers ($N_c(r)$) of the oxygen from the solvent for (a) LiTFSI in tetraglyme, (b) LiFSI in c8-dmc, and (c) LiTFSI in c8-dmc. In each case the results are given for five different concentrations. Dashed lines are the coordination number and solid lines are the $g(r)$.

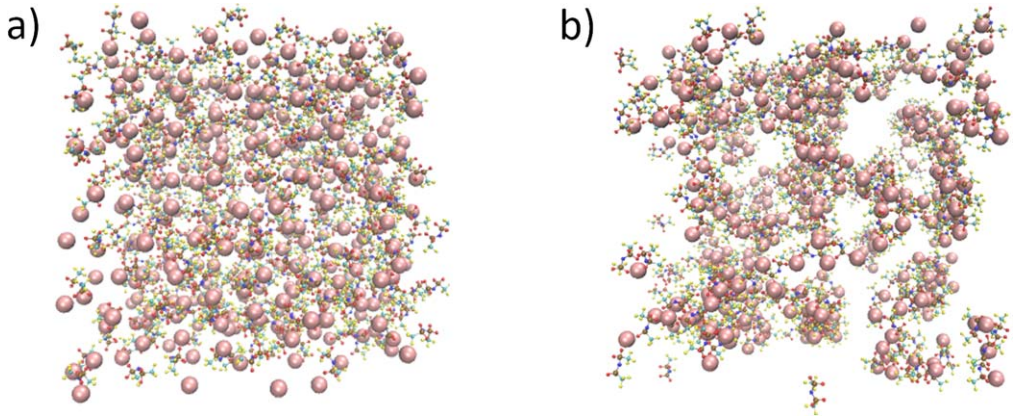

Figure 2. Final snapshot of (a) the tetraglyme (r = [Li]/[O] = 0.14) system and (b) the c8-dmc (r = [Li]/[O] = 0.08) systems or $x_{salt} = 0.24$ for both systems. In both figures, Li are the pink spheres and the ball and stick molecules are TFSI. The tetraglyme and c8-dmc are not shown for clarity.

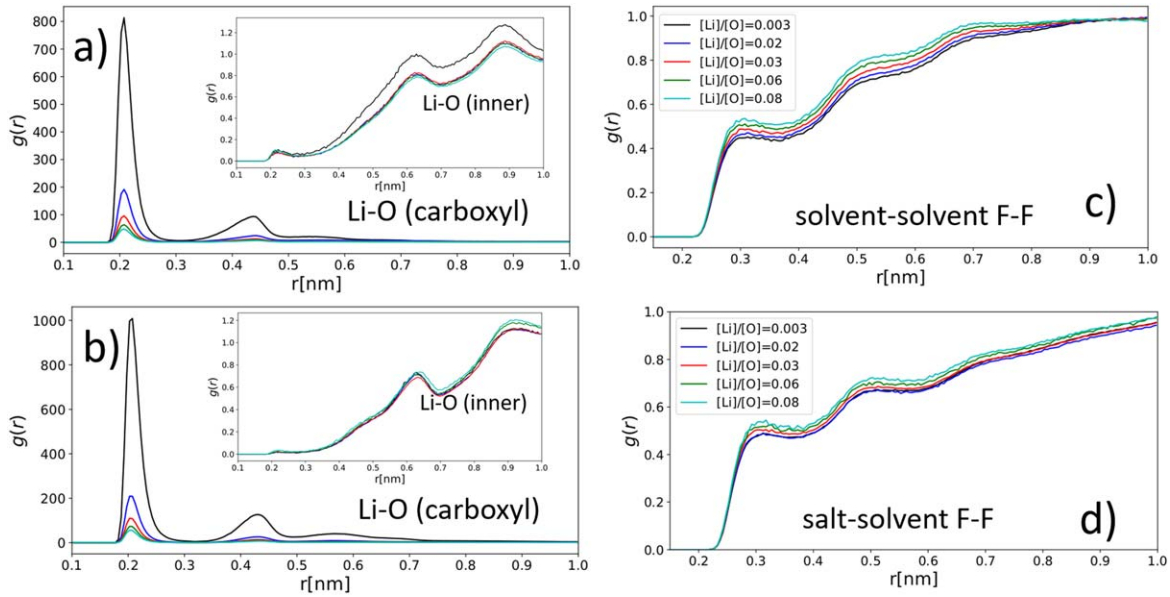

Figure 4. Radial distribution functions *(g(r))* between Li and the O in c8-dmc or the F in c8-dmc and the salt: (a) Li-O for the oxygen in the carboxyl group and the inner oxygen (inset) coordinated with the Li cation for the LiFSI system, (b) Li-O for the oxygen in the carboxyl group and the inner oxygen (inset) coordinated with the Li cation for the LiTFSI system, (c) F-F intermolecular solvent molecules in the TFSI system, (d) F solvent–F anion in the TFSI system. The ratios r = [O]/[Li] = 0.003, 0.02, 0.03, 0.06, and 0.08 are black, blue, red, green, and cyan, respectively.

Table 1. Binding energies, ΔE, in eV, for various species interacting with c8-dmc and triglyme calculated at the B3LYP/6–31 + G(d) level of density functional theory.[a)]

	One-coord.	Two- coord.	Three-coord.	Four-coord.
		c8-dmc		
Li+	1.7 eV	1.8–2.3 (3)	2.4–2.6 (2)	2.6–3.1 (5)
FSI-	.18 to 0.30 (7)	—	—	
LiFSI	0.43 to 0.89 (13)	0.45 to 0.70 (5)	—	
$Li(FSI)_2^-$	.08 to 0.29 (5)			
		Triglyme[b)]		
Li+				4.3
FSI-	.16 to .20			
LiFSI	1.0 to 1.5 (3)	1.5		

a) Numbers in parentheses are the number of different structures investigated. b) Triglyme has similar energetics as tetraglyme. A calculation of the interaction energy of tetraglyme with Li^+ in the four-coordination structure gives 4.2 eV, very similar to the result for tetraglyme.

where h is unity if the salt aggregate is identical to the aggregate at time *t*. A salt aggregate in this calculation is defined by calculating the second neighbors of only the lithium cations for simplicity. The cut-off of the second neighbors is 0.8 nm, chosen from the end of the first peak in the radial distribution function of lithium-lithium interactions (not shown).

Lastly, the conductivity was calculated from the mutual diffusion between the anion and cation, as in the following equation[36]

$$\sigma = \lim_{t\to\infty} \frac{e^2}{6tVk_BT} \sum_{ij}^{N} Z_i Z_j [R_i(t) - R_i(0)][R_j(t) - R_j(0)] \quad [4]$$

where σ is the conductivity, V is the volume of the simulation box, k_B is the Boltzmann constant, T is the temperature, *e* is the elementary charge, Z_i and Z_j are charges of species i and j, and $R_i(t)$, $R_i(0)$ are the unwrapped coordinates at time t and time 0 of species i.

Results and Discussion

We characterized our system with the OPLS force field using bulk simulations of c8-dmc and tetraglyme. The densities of the system were calculated for the bulk chains. The tetraglyme system[37] has a density of 1.01 g cm^{-3}, and the c8-dmc system[7] has a density of 1.51 g cm^{-3}, which both match experimental densities.[7,37]

Local solvation structure.—In Fig. 3, we present the radial distribution function *g(r)* and coordination number n of the Li ion and the oxygen of the chains to provide information on the local structure of the molecules. The coordination number is calculated using equation $n = 4\pi\rho \int_0^{r_c} g(r)dr$, where ρ is the number density of solvent oxygens and $r_c = 0.3$ nm is the cut-off distance. For the tetraglyme molecule, there is a slight decrease in the coordination number of solvent oxygens from n = 5.6 to n = 4.9 as we increased the concentration of the salt, as seen in Fig. 3a, consistent with the work by Molinari et al.[19]). However, there was very little change of the solvent oxygen coordination number (n = 1.41 to n = 1.48) for c8-dmc as we increase the concentration of the salt, as seen in Fig. 3b. The coordination of the lithium with the oxygens of the solvent and salt is four times greater in tetraglyme than c8-dmc. The total oxygen coordination from the anion and solvent is approximately 5.3, which is similar to the tetraglyme system. The low concentration, r = 0.003, has an artificially higher first peak in

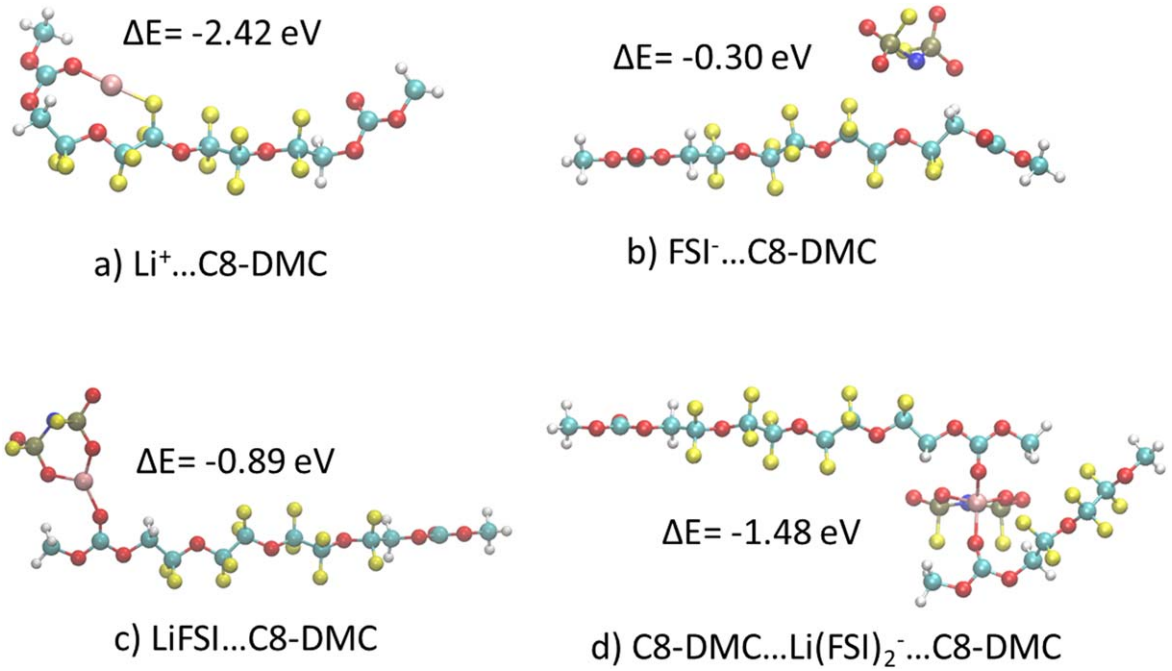

Figure 5. Representative DFT calculated structures for LiFSI salt species interacting with c8-dmc. (a) three coordinated Li^+ - c8-dmc, (b) most stable structure found for FSI anion interacting with c8-dmc, (c) most stable structure found for LiFSI interacting with c8-dmc, (d) structure for LiFSI interacting with two c8-dmc with the second c8-dmc having a shortened chain.

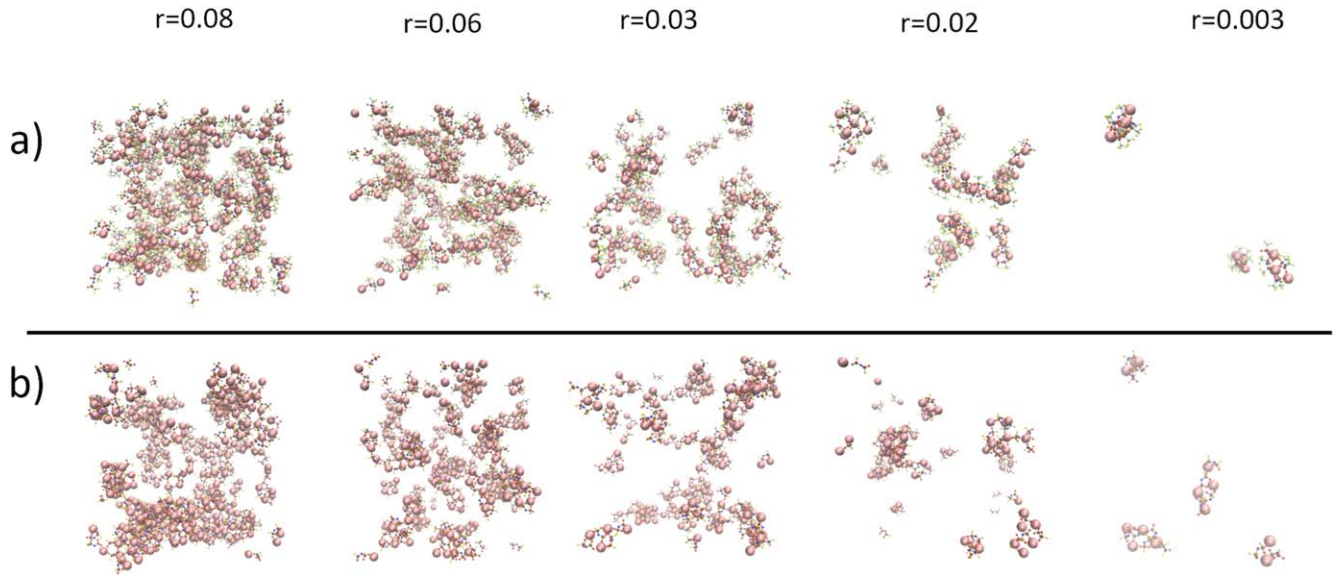

Figure 6. Snapshots of the aggregates for differing concentrations (r = [O]/[Li]) and anions. The systems are (a) LiFSI in c8-dmc and (b) LiTFSI in c8-dmc.

Fig. 3a due to the low concentration and salt aggregation (the salt aggregation will be discussed in detail below).

To verify which atoms of the c8-dmc chains the lithium cations bond to, we examined the radial distributions of the carboxyl oxygens and ether oxygens. In Figs. 4a, 4b, we show the radial distribution of the carboxyl group, indicating a high coordination over these oxygens. The first peak corresponds to the carbonyl oxygen and the second peak around 0.45 nm corresponds to the singly bonded oxygens in the carboxyl group. In Figs. 4a, 4b insets, there is little coordination with the ether oxygens in the middle of the chain. We see that the lithium ions are almost exclusively coordinating with the ends of the chains on the carboxyl groups due to the stronger interaction of the Li with the carbonyl oxygen than the ether oxygens in the middle of the chain. For the tetraglyme chains, every ether oxygen has the same probability of interacting with a lithium cation.

Figure 2b shows a percolating network structure of salts, which we denote as salt aggregates. The aggregation occurs due to the weak solvating power of c8-dmc with salts and the intermolecular fluorine-fluorine interaction in the solvent, the latter of which favors the segregation of some of the solvent molecules. The *g(r)* of F-F interactions of the solvent (Fig. 4c), are similar for each concentration and are very similar for the F-F interaction between the solvent and TFSI (Fig. 4d). The FSI calculations are not shown but are similar. The interaction between the fluorines of the solvent molecules is most likely from a fluorous effect since the closest

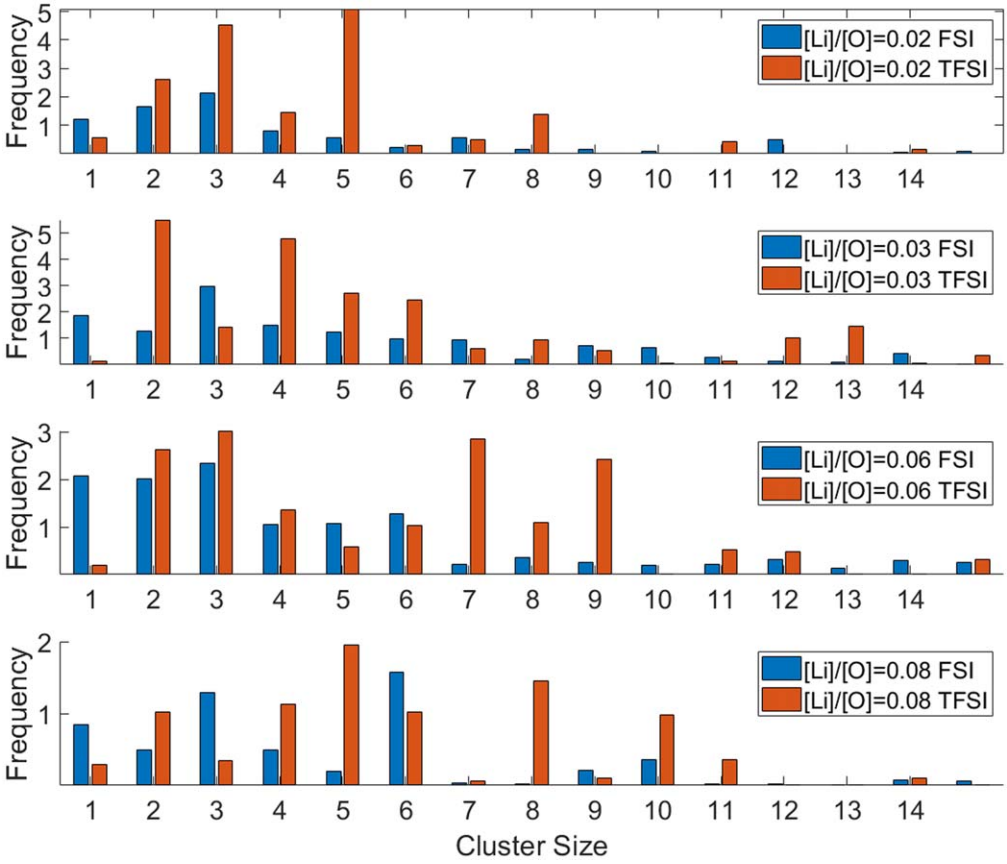

Figure 7. Time-averaged appearance frequency of the number of ionic aggregates for LiTFSI (orange) and LiFSI (blue) in c8-dmc for four concentrations of salts.

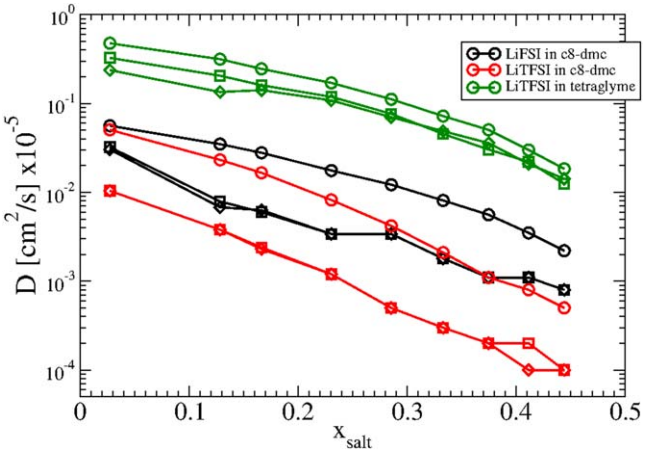

Figure 8. Self-diffusion constants for three systems: LiFSI in c8-dmc (black), LiTFSI in c8-dmc (red), and LiTFSI in tetraglyme (green). The squares are the anion diffusion constants, the diamonds are the Li diffusion constants, and the circles are the solvent molecule diffusion constants.

F–F distances are at 2.8–2.9 Angstroms, and additionally DFT simulations provide a binding energy of 0.9 eV between two solvent molecules at 2.8 Angstroms.[38]

The results for the DFT calculations of the interaction energies of the various salt species (Li^+, FSI^-, LiFSI, and $Li(FSI)_2^-$) with the c8-dmc molecule are given in Table I. Representative structures are given in Fig. 5. Also given in Table I are the interaction energies of various salt species ((Li^+, FSI^-, and LiFSI) with triglyme for comparison with c8-dmc. The interaction energies for Li^+ range from 1.7 to 3.1 eV for one to four-coordination of Li^+ with the solvent, and the four-coordination configurations are shown in Fig. S4 (available online at stacks.iop.org/JES/169/020506/mmedia). The most stable four-coordination binding energy of 3.1 eV (Fig. S4a) for c8-dmc is weaker than that for triglyme four-coordination, which is 4.3 eV. This is consistent with the effect of the fluorine weakening the interaction with the salt as discussed above. The results for the FSI anion in Table I for both systems indicate a very weak interaction of 0.1 to 0.3 eV. The $Li(FSI)_2$ anion also has a very weak interaction. The calculations for the LiFSI interaction in Table I indicate that it is stronger for triglyme by about a factor of two than for c8-dmc, consistent with the stronger interaction found for the Li cation in the DFT calculations and the fluorine effect found in the MD simulations. The DFT result for the structure of LiFSI interacting with c8-dmc is also consistent with the MD simulations as the most stable structures among the 13 that we investigated have the LiFSI bonded to the carbonyl group of the c8-dmc as opposed to an ether group in the center of the chain. An example of such a structure is given in Fig. 5c as well as one with LiFSI bonded to two chains in Fig. 5d. In addition, the energies in Table I also provide insight into why aggregation occurs in c8-dmc, which is that the salt has a weaker interaction with the c8-dmc. This weaker interaction could be the driving force for the aggregation of the salt over the homogeneous distribution found for tetraglyme.

Aggregate structures.—Figure 6 shows snapshots for varying concentrations of salt in c8-dmc, showing the different appearances of aggregates. Visually, the aggregates are transient and change as the simulations progress. The structures of the salt aggregates can be analyzed in various ways, but we implement the cluster analysis from Yu et al.[34] The time-averaged appearance frequency histogram of the aggregates of different sizes are plotted for both salts in Fig. 7, averaged over 500 ns. The aggregates are neutral in these systems

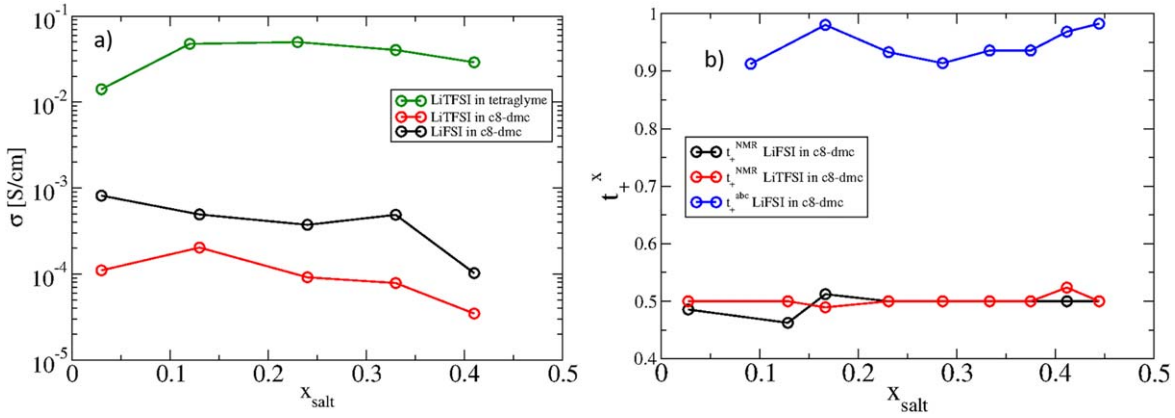

Figure 9. (a) Conductivity of the three systems: tetraglyme with LiTFSI in green, c8-dmc with LiFSI in black, and c8-dmc with LiTFSI in red. The lines are plotted to guide the eyes. (b) The transference number from self-diffusions, t_+^{NMR} for LiFSI in c8-dmc (black) and LiTFSI in c8-dmc(red), and from the Rolling Method, t_+^{abc} for LiFSI in c8-dmc (blue).

and we show the frequency histogram vs the number of lithium cations in the aggregate. A cluster size of one has one Li and at least one anion, which is essentially an ion pair; while a cluster size of two, contains two Li cations with a variety of oxygens from the anion, and so on. There is a larger probability for smaller aggregate sizes for LiFSI and larger aggregate sizes for LiTFSI as shown in Fig. 7.

We calculate the lifetime of the salt aggregates following the work done by Keith et al.[39] and Borodin and Smith[37] to understand the transient nature of the salt aggregates. We calculate the mean residence time, τ_{res}, of the Lithium cation aggregates from fitting the correlation function to an exponential $C(t) = c + Ae^{-t/\tau_{res}}$. For the LiFSI system, τ_{res} = 232 ns, 229 ns, 263 ns, and 258 ns for r = [Li/O] = 0.02, 0.03, 0.06, and 0.08 respectively. For the LiTFSI system τ_{res} = 1020 ns, 436 ns, 290 ns, and 246 ns for the same concentrations as before. The residence time calculations show the salt aggregates in the LiFSI system are more short-lived compared to the LiTFSI system, but as the concentration increases the lifetimes of the aggregates approach approximately the same value. Zhang and Maginn[40] calculated ion pair lifetimes for a large number of ion pairs, and their lifetimes are approximately 10^3 times shorter than the lifetime of these Li cation clusters, which shows how long lived these aggregates are.

Dynamics.—To further understand the dynamics, we examine the self-diffusion of the chains, cations, and anions. The self-diffusion constant of the chains as a function of concentration is seen in Fig. 8. A comparison of these results with experimental values can be found in Fig. S5. As expected, the chains slow down when there is an increase in the number of ions. In the tetraglyme system, the Li cations move faster than the anion and solvent molecules as expected at higher concentrations, but the anion moves the slowest. For c8-dmc, however, the cation and anion move together, a function of the aggregation of the Li cations. The c8-dmc molecules diffuse faster than the ions, which is also seen in Grundy et al.[7] Our self-diffusion calculations match nicely with the experimental data in Grundy et al.[7] (Fig. S5).

The calculated conductivity, as seen in Fig. 9a, matches experimental data qualitatively for c8-dmc,[7] but the conductivity of tetraglyme matches both experimentally and previous simulations.[10,37] The plot shows tetraglyme with LiTFSI to have the highest conductivity, while the next highest is c8-dmc with LiFSI, followed by c8-dmc with LiTFSI. Combining the diffusion and cluster analysis data, we can see that the transient aggregates of the c8-dmc LiFSI have a more significant effect on the diffusion and conductivity of the system. Lastly, the ionicities of the electrolytes, which reflect the degree of uncorrelated motion in the systems, are presented in Fig. S6. The ionicity results show that the ion motion in the c8-dmc electrolytes becomes highly correlated at the highest concentration.

The transference number is vital to understanding polymer electrolytes and the NMR transference number (t_+^{NMR}) can be calculated by the self-diffusion values, $t_+^{NMR} = D_+/(D_- + D_+)$, where D_+ and D_- are the self-diffusion coefficient of cation and anion, respectively. The transference numbers calculated using this method for the systems are approximately 0.5 and invariant with concentration, as shown in Fig. 9b, due to the negligence of the ion correlation. We also calculated correlated transference numbers using a relatively simple method presented Dong et al.[41] We first reproduced the values of α, β, and t_+^{abc} for the tetraglyme system as in their paper (results in supplemental information). The results for c8-dmc system are presented in Fig. 9b and we see that the correlated transference number (t_+^{abc}) is close to one for all salt concentrations. These results are very different from the t_+^{NMR} calculated based on self-diffusion, indicating that the inclusion of ion correlation has a significant effect on the t_+ calculations.

The calculated t_+^{abc} are also quite different from those of Grundy et al.,[7] even though the same simulation approach has been shown to be sufficient for many highly correlated systems. From Grundy et al., the solvent plays an important role in the transference number (t_0^+) based on the concentrated solution theory and the cation-anion diffusion is the dominating factor in the conductivity for c8-dmc. Therefore, methods such as those based on Stefan-Maxwell diffusion that captures the solvent effect with ion correlation may yield better agreement with the transference numbers in the experimental work. The implementation of such methods is nontrivial and will be the subject of our future studies.

Conclusions

Here, we explored the structural and dynamic properties c8-dmc and tetraglyme with two different lithium salts (FSI and TFSI). These results provide evidence that the fluorine on the chains is blocking the Li cation's interaction with oxygens on the c8-dmc chain. The Li cation interacts only with the end of the chain. An aggregation of salt molecules occurs due to the weak solvating power of c8-dmc with salts and the intermolecular fluorine-fluorine interaction in the solvent, the latter of which favors the segregation of some of the solvent molecules. However, in the tetraglyme system, the Li cation interacts throughout the chain. We used DFT calculations to show the energetics of the systems, verifying the location of the salts is energetically favorable. Comparing the aggregates of Li with differing salts (FSI and TFSI) in c8-dmc showed that these salts change the size and shape of aggregation in the system. Using a time-averaged frequency map and a lifetime analysis, we can see that TFSI has larger and less transient aggregates.

We also examined the self-diffusion and conductivity of the systems. The self-diffusion of all three systems is consistent with

the experimental results of Grundy et al.[7] Although the tetraglyme conductivity calculations matched experiments and simulation,[17,36,37] the simulations with LiFSI/TFSI in c8-dmc showed a higher conductivity for LiFSI compared to LiTFSI, but while the trend matched experimental conductivity data,[7,23] the magnitude of the conductivity was off by a factor of 10. The mechanism leading to a higher conductivity in the LiFSI system was not investigated, but further calculations involving more precise techniques such as mutual diffusion and cluster transport algorithms will be used in future work[17,36,37] to help elucidate the effect of aggregation on conductivity.

Acknowledgments

This research was supported by the Joint Center for Energy Storage Research (JCESR), a U.S. Department of Energy, Energy Innovation Hub. The submitted manuscript has been created by UChicago Argonne, LLC, Operator of Argonne National Laboratory ("Argonne"). Argonne, a U.S. Department of Energy Office of Science laboratory, is operated under contract no. DE-AC02–06CH11357. We thank the Laboratory Computing Resource Center at Argonne National Laboratory for the generous allocation of computing time on the Bebop cluster.

ORCID

Zhou Yu https://orcid.org/0000-0003-3316-4979
Lei Cheng https://orcid.org/0000-0002-3902-1680

References

1. K. Jorgensen, *Util. Policy*, **16**, 72 (2008).
2. Z. Zhang, L. Hu, H. Wu, W. Weng, M. Koh, P. C. Redfern, L. A. Curtiss, and K. Amine, *Energy Environ. Sci.*, **6**1806 (2013).
3. R. Eisenberg, H. B. Gray, and G. W. Crabtree, *PNAS*, **117**, 12541 (2020).
4. M. U. Ali, A. Zafar, S. H. Nengroo, S. Hussain, M. J. Alvi, and H.-J. Kim, *Energies*, **12**, 446 (2019).
5. D. Aurbach, *J. Power Sources*, **89**, 206 (2000).
6. Y. Choo, D. M. Halat, I. Villaluenga, K. Timachova, and N. P. Balsara, *Prog. Polym. Sci.*, **103**, 101220 (2020).
7. L. S. Grundy, D. B. Shah, H. Q. Nguyen, K. M. Diederichsen, H. Celik, J. M. DeSimone, B. D. McCloskey, and N. P. Balsara, *J. Electrochem. Soc.*, **167**, 120540 (2020).
8. D. T. Hallinan and N. P. Balsara, *Annu. Rev. Mater. Res.*, **43**, 503 (2013).
9. Y. M. Lin, K. C. Klavetter, P. R. Abel, N. C. Davy, J. L. Snider, A. Heller, and C. B. Mullins, *Chem. Commun.*, **48**, 7268 (2012).
10. D. B. Shah, K. R. Olson, A. Karny, S. J. Mecham, J. M. DeSimone, and N. P. Balsara, *J. Electrochem. Soc.*, **164**, A3511 (2017).
11. C. V. Amanchukwu, Z. Yu, X. Kong, J. Qin, Y. Cui, and Z. Bao, *J. Am. Chem. Soc.*, **142**, 7393 (2020).
12. K. R. Olson, D. H. C. Wong, M. Chintapalli, K. Timachova, R. Januszewicz, W. F. M. Daniel, S. Mecham, S. Sheiko, N. P. Balsara, and J. M. DeSimone, *Polymer*, **100**, 126 (2016).
13. X. Fan et al., *Nat. Energy*, **4**, 882 (2019).
14. X. Fan et al., *Chem*, **4**, 174 (2018).
15. S. Sawayama, Y. M. Todorov, H. Mimura, M. Morita, and K. Fujii, *Phys. Chem. Chem. Phys.*, **21**, 11435 (2019).
16. F. L. Celso, G. B. Appetecchi, E. Simonetti, U. Keiderling, L. Gontrani, A. Triolo, and O. Russina, *J. Mol. Liq.*, **289**, 111110 (2019).
17. A. France-Lanord and J. C. Grossman, *Phys. Rev. Lett.*, **122**, 136001 (2019).
18. M. Bernardi, P. Marracino, M. Liberti, J. A. Garate, C. J. Burnham, F. Apollonio, and N. J. English, *Phys. Chem. Chem. Phys.*, **21**, 3339 (2019).
19. N. Molinari, J. P. Mailoa, and B. Kozinsky, *Chem. Mater.*, **30**, 6298 (2018).
20. N. Molinari and B. Kozinsky, *J. Phys. Chem. B*, **124**, 2676 (2020).
21. D. Shivakumar, J. Williams, Y. Wu, W. Damm, J. Shelley, and W. Sherman, *J. Chem. Theory Comput.*, **6**, 1509 (2010).
22. B. Doherty, X. Zhong, S. Gathiaka, B. Li, and O. Acevedo, *J. Chem. Theory Comput.*, **13**, 6131 (2017).
23. D. B. Shah, H. Q. Nguyen, L. S. Grundy, K. R. Olson, S. J. Mecham, J. M. DeSimone, and N. P. Balsara, *Phys. Chem. Chem. Phys.*, **21**, 7857 (2019).
24. J. S. Smith, O. Borodin, G. D. Smith, and E. M. Kober, *J. Polym. Sci., Part B: Polym. Phys.*, **45**, 1599 (2007).
25. H. J. C Berendsen, D. van der Spoel, and R. van Drunen, "GROMACS: A message-passing parallel molecular dynamics implementation." *Comp. Phys. Comm.*, **91**, 43 (1995).
26. W. L. Jorgensen and J. Tirado-Rives, *PNAS*, **102**, 6665 (2005).
27. R. W. Hockney and J. W. Eastwood, *Computer Simulation Using Particles* (CRC Press, Boca Raton) (1988).
28. G. Bussi, D. Donadio, and M. Parrinello, *J. Chem. Phys.*, **126**, 014101 (2007).
29. M. Parrinello and A. Rahman, *J. Appl. Phys.*, **52**, 7182 (1981).
30. M. P. Allen and D. J. Tildesley, *Computer Simulation of Liquids* Second Edition ed. (Claredon Press, Oxford) (1987).
31. U. Essmann, L. Perera, M. L. Berkowitz, T. Darden, H. Lee, and L. G. Pedersen, *J. Chem. Phys.*, **103**, 8577 (1995).
32. M. J. Frisch, G. W. Trucks, H. B. Schlegel, G. E. Scuseria, M. A. Robb, J. R. Cheeseman, G. Scalmani, V. Barone, G. A. Petersson, and H. Nakatsuji et al., (2016), Gaussian, Inc., Wallingford CT.
33. B. Everitt, S. Landau, M. Leese, and D. Stahl, *Cluster Analysis* (Wiley, New York, NY) (2011).
34. Z. Yu, L. A. Curtiss, R. E. Winans, Y. Zhang, T. Li, and L. Cheng, *The Journal of Physical Chemistry Letters*, **11**, 1276 (2020).
35. O. Borodin, G. D. Smith, and W. Henderson, *J. Phys. Chem. B*, **110**, 16879 (2006).
36. D. Dong and D. Bedrov, *J. Phys. Chem. B*, **122**, 9994 (2018).
37. O. Borodin and G. D. Smith, *Macromolecules*, **39**, 1620 (2006).
38. R. Berger, G. Resnati, P. Metrangolo, E. Weber, and J. Hulliger, *Chem. Soc. Rev.*, **40**, 3496 (2011).
39. J. R. Keith, S. Mogurampelly, B. K. Wheatle, and V. Ganesan, *J. Polym. Sci., Part B: Polym. Phys.*, **55**, 1718 (2017).
40. Y. Zhang and E. J. Maginn, *The Journal of Physical Chemistry Letters*, **6**, 700 (2015).
41. D. Dong, F. Salzer, B. Roling, and D. Bedrov, *Phys. Chem. Chem. Phys.*, **20**, 29174 (2018).